Chemical Science

ROYAL SOCIETY OF CHEMISTRY

EDGE ARTICLE

View Article Online
View Journal

Cite this: DOI: 10.1039/d5sc06987d

All publication charges for this article have been paid for by the Royal Society of Chemistry

Received 10th September 2025
Accepted 4th December 2025

DOI: 10.1039/d5sc06987d

rsc.li/chemical-science

Asymmetric vicinal C(sp^3)–H difunctionalization of saturated cyclic amines *via* synergistic photoredox, copper and chiral phosphoric acid catalysis

Teng-Fei Xiao,[a] Ke-Rui Jian,[a] Yu-Cheng Gu,[b] Guo-Qiang Xu *[a] and Peng-Fei Xu *[a]

Existing strategies are typically limited to modifying a C–H site (α or β-position) of saturated cyclic amines, but the asymmetric difunctionalization of vicinal C–H bonds remains a formidable challenge. To address this challenge, this work introduces a synergistic catalytic system that merges visible-light photocatalysis with asymmetric copper and chiral phosphoric acid catalysis. This system enables the enantioselective synthesis of ring-fused amine skeletons by activating vicinal C–H bonds in straightforward saturated cyclic amines. The reaction proceeds in good yields (up to 76%) and excellent enantioselectivity (up to 92% ee). This work describes detailed mechanistic studies that identify the specific dual chiral catalytic system that forms the basis for the enantioselectivity.

Introduction

Nitrogen-containing heterocyclic rings are crucial structural motifs in natural products and pharmaceuticals.[1–3] The direct conversion of readily available saturated cyclic amines into high-value-added chiral compounds *via* C(sp^3)–H functionalization has attracted significant interest from both academic and industrial researchers. Driven by its inherent atom- and step-economy and facilitated by the abundant availability of precursors, this approach represents a promising and transformative strategy in synthetic chemistry. However, achieving enantioselective C(sp^3)–H functionalization of saturated cyclic amines remains a long-standing challenge in asymmetric catalysis. In recent years, several particularly attractive strategies have emerged for the α-functionalization of these amines with high enantioselectivity, including metal/chiral ligand catalysis, chiral phosphoric acid (CPA) catalysis, and enzymatic α-functionalization (Fig. 1b).[4–6] Despite the significant advancements in this field, most methods primarily facilitate the transformation of one C–H bond, while numerous synthetic endeavors necessitate the installation of multiple functional groups. Consequently, reactions capable of asymmetrically functionalizing multiple C–H bonds remain less explored, despite their potential to enable highly efficient and concise synthetic routes.[7,8]

Among various aza-cycles, cyclic amines represent a fundamental scaffold.[9] Notably, ring-fused amine skeletons serve as fundamental structures in numerous natural products and pharmaceuticals.[10–14] For instance, compounds featuring this skeleton have shown promise in the prevention and treatment of Alzheimer's disease, as evidenced by a granted Chinese patent (Fig. 1a).[15–17] In addition, (*S*)-blebbistatin is a well-characterized ATPase inhibitor that selectively targets myosin II.[18] Due to their intriguing structure and potentially beneficial biological properties, the synthesis of ring-fused amine skeletons has garnered significant interest within the synthetic community.[19–22]

Despite the progress in the field, the synthesis of ring-fused amine skeletons still largely relies on labor-intensive *de novo* synthesis.[23] We propose that constructing ring-fused amine skeletons through activation of vicinal C–H bonds in simple saturated cyclic amines would significantly streamline the synthetic route. This approach inherently introduces chirality—a critical factor for the pharmacological efficacy of drug molecules. However, compared to the installation of a single stereocenter, the difunctionalization of vicinal C–H bonds poses significant challenges in controlling regioselectivity, diastereoselectivity, and enantioselectivity (Fig. 1c). When a single chiral catalyst proves insufficient to address these issues, a dual catalytic system becomes necessary. Herein, we report the first enantioselective synthesis of ring-fused amine skeletons *via* visible-light photocatalytic activation of vicinal C–H bonds in saturated cyclic amines (Fig. 1d). Crucially, high enantioselectivity is achieved through a synergistic catalysis mechanism involving hydrogen bonding between the chiral phosphoric acid and the substrate, complemented by an additional counteranion interaction with the chiral copper cation.

[a]*State Key Laboratory of Natural Product Chemistry, College of Chemistry and Chemical Engineering, Lanzhou University, Lanzhou 730000, Gansu, China. E-mail: xupf@lzu.edu.cn; gqxu@lzu.edu.cn*

[b]*Syngenta Jealott's Hill International Research Centre, Bracknell, Berkshire, RG42 6EY, UK*

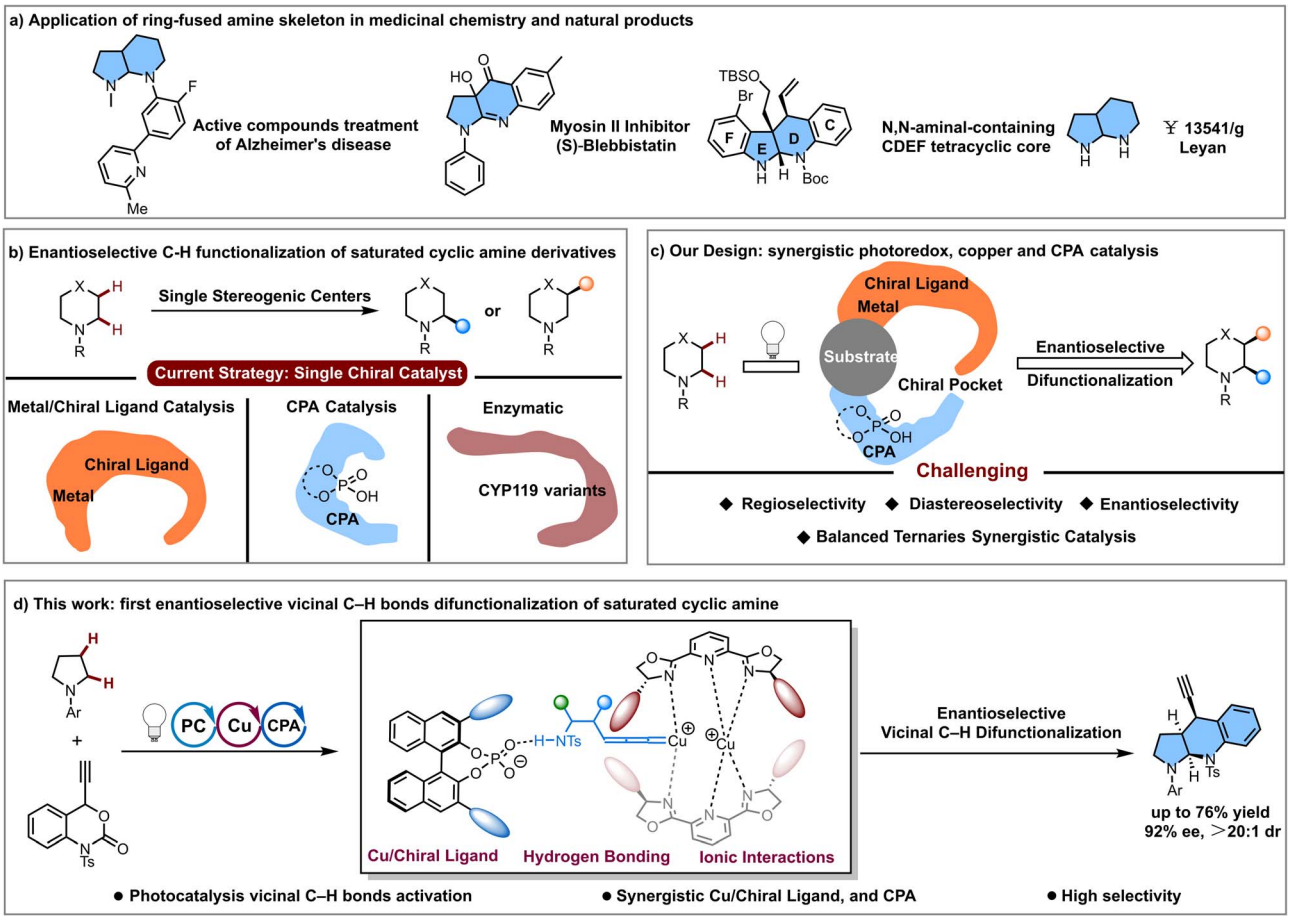

Fig. 1 Enantioselective vicinal C(sp^3)–H difunctionalization of saturated cyclic amines. (a) Application of ring-fused amine skeletons in medicinal chemistry and their presence in natural products. (b) Previous strategies to achieve stereocontrol of saturated cyclic amines by single chiral catalysis. (c) Our design of synergistic photoredox, copper, and chiral phosphoric acid catalysis. (d) Development of enantioselective vicinal C(sp^3)–H difunctionalization of saturated cyclic amines.

Results and discussion

Reaction optimization

We initially investigated the asymmetric vicinal C–H bond functionalization between *N*-phenyl pyrrolidine **1a** and propargylic carbamate **2a** using a catalytic system comprising CuI (10 mol%), chiral ligand **L-1** (12 mol%), and ^{t}Bu-DCQ (1 mol%) in the presence of pentafluoronitrobenzene (PFNB, 0.5 equiv.) and $NaHCO_3$ (2.0 equiv.) in THF under white LED irradiation. Under these conditions, the desired product **3a** was obtained in 11% yield with 55% ee. Switching to other commonly employed photocatalysts resulted in the formation of trace products. To improve the enantioselectivity, we next examined several chiral ligands with varying structural frameworks. After evaluation, tridentate chiral PyBox ligands proved optimal. Among them, ligand **L-1** afforded the product in moderate yield and enantioselectivity. Further modifications to the ligand revealed that increasing the steric bulk from phenyl to naphthyl significantly enhanced enantioselectivity, demonstrating the importance of bulky substituents in stereochemical control. Subsequent evaluation of BOX ligands with varying substituents identified **L-16** as the optimal ligand, likely due to its favorable bite angle (Table 1, see the SI for experimental details).

Unfortunately, systematic modification of the ligand structure did not lead to any significant improvement in either the reaction yield or ee. When a single ligand fails to provide sufficient stereochemical control, we propose introducing a chiral catalyst that can interact with the substrate through hydrogen bonds.[24] Additionally, the counteranion interaction with the chiral copper cation could enhance enantioselective control. Subsequent screening of various chiral hydrogen-bonding catalysts revealed that a chiral phosphoric acid proved to be effective. Guided by this insight, we tested combinations of CuI-**L-16** with various CPAs. The combination of (*R*)-**L-16** and (*R*)-CPA **B-3** yielded the best results, delivering a product with 90% ee. The ee is sensitive to the substituents at the 2,4,6-positions of BINOL. Under optimized conditions—using ^{t}Bu-DCQ (1 mol%), CuI (10 mol%), **L-16** (12 mol%), CPA **B-3** (20 mol%) as catalysts, PFNB (0.35 equiv.), 2 equivalents of $NaHCO_3$ as a base, and 4 Å MS in 1 mL of THF under white LED irradiation at room temperature for 21 hours under an argon atmosphere—the desired product **3a** was obtained in 76% yield with 92% ee with >20 : 1 dr. Notably, no ring-opening byproducts

Table 1 Optimization of the ligand and CPA[a]

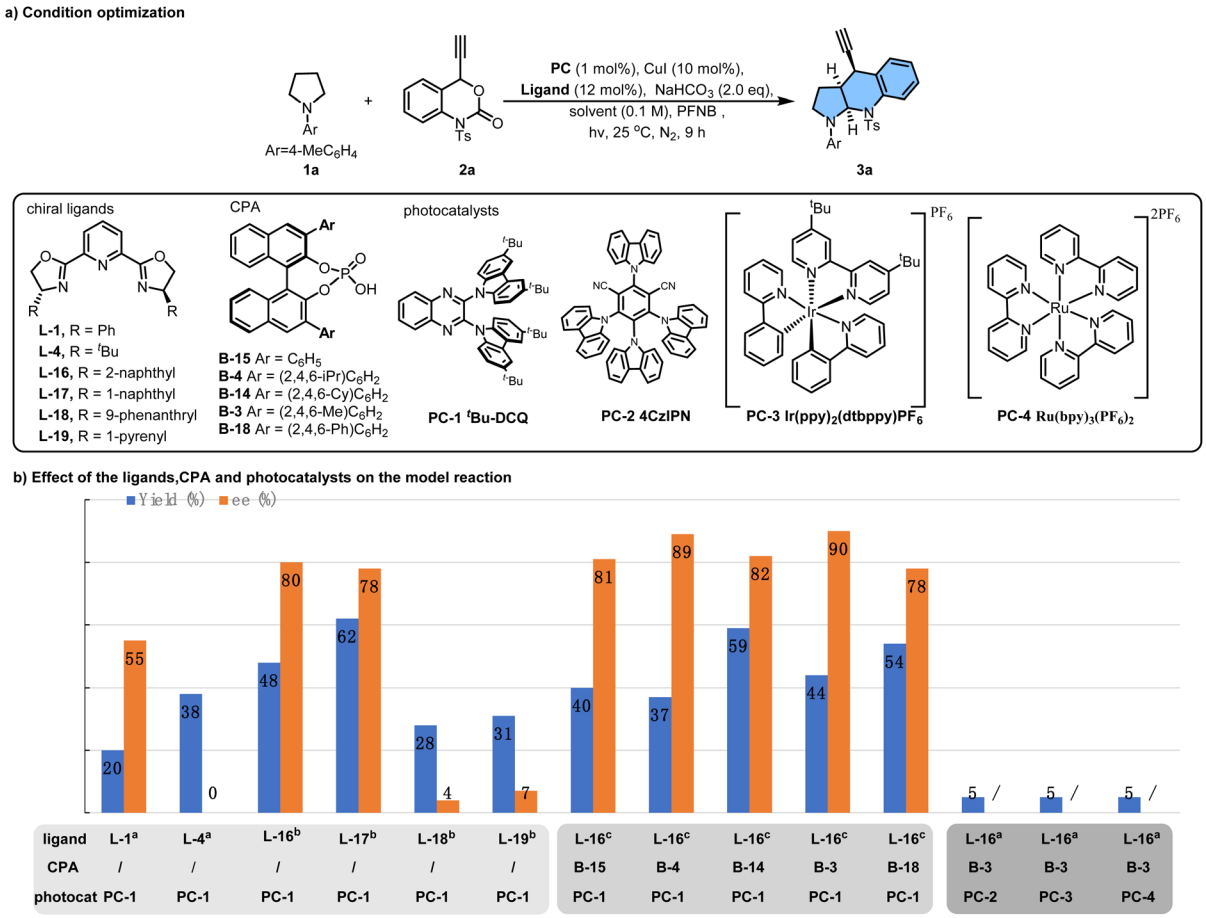

[a] Reaction conditions: **1a** (0.05 mmol), **2a**, $NaHCO_3$ (2 equiv.), PC (1 mol%), PFNB, solvent (0.1 M), and N_2 atmosphere. Isolated yields. ee values were based on chiral HPLC analysis, with >20 : 1 dr based on ^1H NMR analysis. [a]**2a** (1.0 equiv.), ^{t}Bu-DCQ (1 mol%), PFNB (0.5 equiv.), and DCM (0.1 M). [b]**2a** (1.6 equiv.), ^{t}Bu-DCQ (1 mol%), THF (0.1 M), and PFNB (0.5 equiv.). [c]**2a** (1.6 equiv.), ^{t}Bu-DCQ (1 mol%), PFNB (0.35 equiv.), **L-16** (12 mol%), 4 Å MS (5 mg), CPA (10 mol%), and ^{t}Bu-DCQ (1 mol%) in THF (1 mL).

were detected, highlighting the high chemoselectivity of the reaction.

Substrate scope

With the optimized reaction conditions in hand, we explored the substrate scope of enantioselective vicinal C(sp^3)–H difunctionalization (Table 2). A variety of saturated aza-heterocycles bearing different *para*-substituents were evaluated (**3a–3f**). Both electron-donating and electron-withdrawing substituents performed well, yielding products with comparable efficiency, although the substitution pattern significantly influenced stereoselectivity. For instance, substrates with 2-naphthyl and 1-naphthyl groups (**3g** and **3h**, reaction conditions B) afforded the desired products in moderate yields with 90–91% ee. Substrates bearing *ortho*- and *meta*-substituents (**3i–3l**, reaction conditions B and C) also underwent the reaction smoothly, although the yields were significantly lower, indicating that *para*-substituents favorably impact the reaction process. Additionally, the protocol enabled access to polysubstituted products (*e.g.*, **3m**, **3n**, **3o**, and **3p**), albeit with moderate enantioselectivity. These results demonstrate the broad applicability of the optimized conditions while highlighting the importance of substituent positioning in achieving high efficiency and selectivity. Compared with pyrrolidine substrates (with a 5-membered ring), the lack of reactivity of piperidine substrates (with a 6-membered ring) is mainly due to the significantly higher oxidation potential of the piperidine nitrogen (see the SI for unsuccessful substrates). The substrate scope was further explored with various ethynyl benzoxazinanone derivatives (Table 2). Introducing substituents at different positions on the benzoxazinanone moiety yielded excellent reaction partners, producing products with high enantioselectivities ranging from 75% to 90% ee. Notably, the stereoselectivity exhibited a subtle dependence on the substituent pattern. For example, substrates **4b**, **4e**, and **4g**, bearing chloro-substituents at the 5-, 6-, and 7-positions, respectively, participated in the reaction smoothly, delivering products with moderate enantioselectivities of 76–83% ee. Bromo-substituted derivatives **4f** and **4h**, with substituents at the 6- and 7-positions, also demonstrated excellent reactivity under the optimized conditions. Additionally, electron-

Table 2 The substrate scope of saturated aza-heterocycles and propargylic carbamates[a,b,c,d,e]

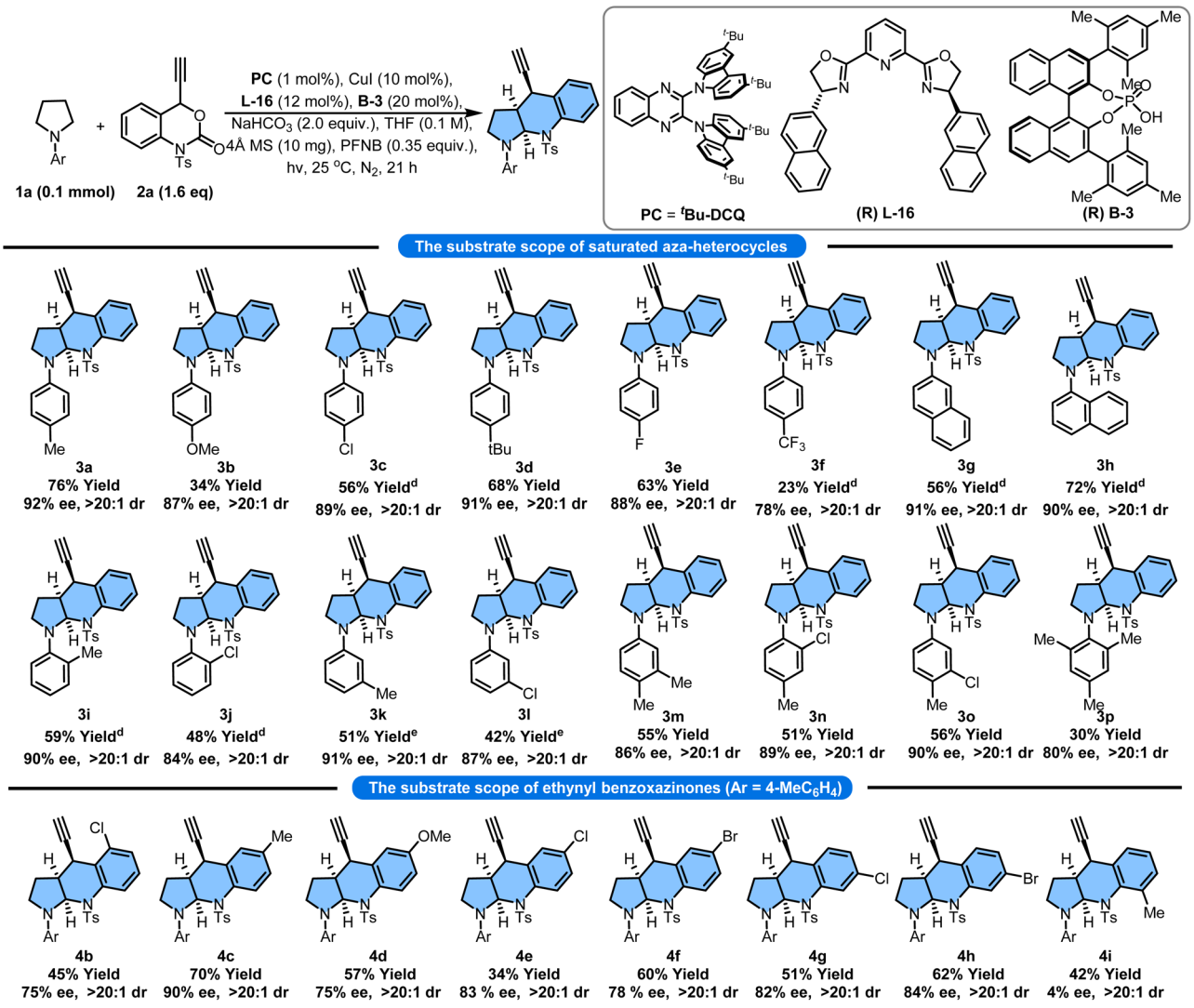

[a] Reaction conditions A: **1a** (0.10 mmol), **2a** (0.16 mmol), ^{t}Bu-DCQ (1 mol%), CuI (10 mol%), **L-17** (12 mol%), CPA **B-3** (20 mol%), $NaHCO_3$ (2 equiv.), PFNB (0.35 equiv.), THF (1 mL), 4 Å MS (10 mg), N_2 atmosphere, and 21 h. [b] Isolated yields. [c] ee values were based on chiral HPLC analysis. [d] Reaction conditions B: ^{t}Bu-DCQ (2 mol%), $NaHCO_3$ (4 equiv.), and 30 h. [e] Reaction conditions C: ^{t}Bu-DCQ (2 mol%), $NaHCO_3$ (4 equiv.), and 48 h.

donating substituents such as methyl group and methoxy groups positioned at the same locations on the aromatic ring (*e.g.*, substrates **4c** and **4d**) were successfully employed in the reaction. These derivatives afforded products in moderate yields and good enantioselectivities, showcasing the method's robustness with a range of substituent types. Furthermore, using the substrate 6-ethynyl-3-tosyl-1,3-oxazinan-2-one did not yield any observable formation of the desired product. For the examples with low enantioselectivity shown in Table 2, we specifically tested the reaction at 0 °C. Regrettably, the enantioselectivity remained largely unchanged, while the yield significantly decreased. However, the 8-methyl-substituted substrate **2i** proved to be a poor substrate, affording **4i** in only moderate yield and with 4% ee, presumably due to steric effects.

Scale-up reaction and functional group transformations

To showcase the applicability of this method, reaction of **1a** with **2a** was performed on a 1 mmol scale under the optimized conditions. The reaction afforded cyclization product **3a** in 45% yield, with excellent stereoselectivity (dr > 20 : 1) and 92% ee (Table 3a).

The resulting product was used for subsequent transformations to highlight the method's versatility (Table 3b). Treatment of **3a** with Mg powder in MeOH at room temperature cleaved the N–Ts bond, yielding compound **5** in moderate yield without compromising the optical purity. The alkyne group in **3a** was hydrogenated using Pd/C, furnishing compound **6** in 86% yield and 89% ee. A Sonogashira coupling reaction

Table 3 Scale-up reaction and functional group transformations of **3a**

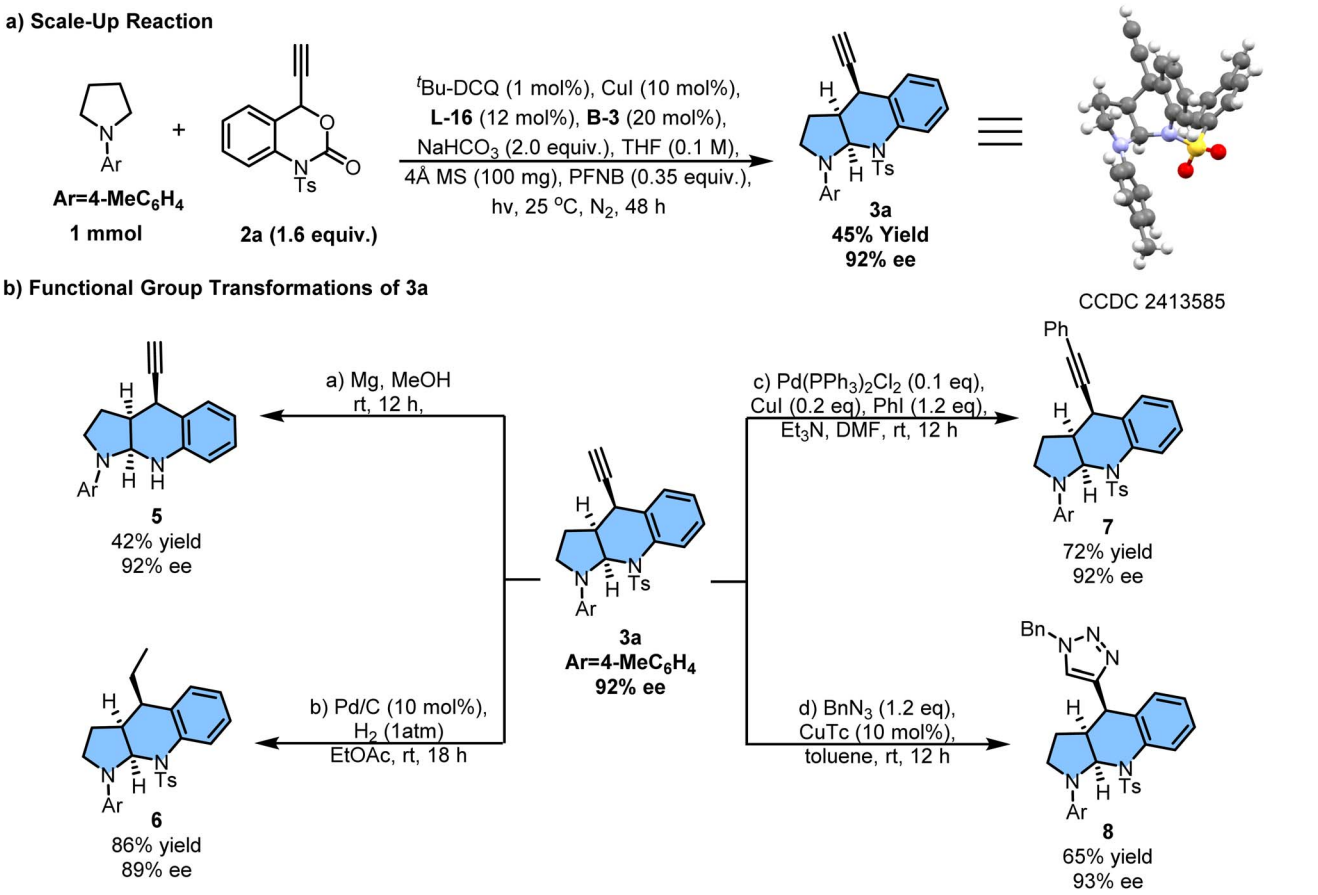

between **3a** and iodobenzene afforded compound **7** in 72% yield and 92% ee, demonstrating the product's ability to participate in palladium-catalyzed cross-coupling reactions. A copper-catalyzed reaction between **3a** and BnN_3 led to the formation of 1,2,3-triazole **8**, obtained in 65% yield while retaining the enantiopurity of the starting material. These transformations highlight the potential of the cyclization product as a versatile intermediate for further functionalization, showcasing its utility in the synthesis of structurally and functionally diverse molecules.

Mechanistic studies

To gain insights into the reaction pathway, a series of mechanistic studies was conducted. Luminescence quenching experiments were performed to verify the initial single-electron transfer (SET) step in the photoredox catalytic cycle. Key findings included: **1a**, PFNB, and **2a** were capable of quenching the excited photocatalyst (^{t}Bu-DCQ); reductive quenching of ^{t}Bu-DCQ by cyclic amine **1a** proceeded at a faster rate than PFNB, indicating that the reaction primarily follows a reductive quenching mechanism (Fig. 2A). Moreover, we unraveled a considerable positive non-linear effect (NLE) in the presence of ligand **L-16** under the optimized reaction conditions. This result indicates that a dinuclear complex of copper salts and the chiral ligand may function as an active catalytic species to promote this transformation, according to previous studies[25] (Fig. 2B). To investigate the rate-limiting step of the transformation, kinetic isotope effect (KIE) experiments were conducted under standard conditions using deuterated substrates: $\mathbf{d_{4\alpha}}$**-1a**, $\mathbf{d_{4\beta}}$**-1a**, and $\mathbf{d_8}$**-1a** yielded KIE values of 1.94 : 1, 2.26 : 1, and 2.47 : 1, respectively (Fig. 2C). The similar kinetic isotope effect (KIE) values for the cleavage of the α- and β-C(sp^3)–H bonds (both ~2) are insufficient to conclusively determine the rate-limiting step. DFT calculations have also been carried out to provide evidence (detailed information is available in the SI). We conducted *in situ* ^{31}P NMR studies to identify chiral phosphoric acid (CPA-**B-3**) species participating in the asymmetric catalytic cycle.[26] Initial characterization of CPA in $CDCl_3$ revealed single resonances at δ = 2.95 ppm. Subsequent neutralization with $NaHCO_3$ induced the complete disappearance of the CPA signal, concomitant with the emergence of a new single resonance (δ = 1.53 ppm) corresponding to phosphate formation. Intriguingly, further addition of CuI, **L-16**, and **2a** (*in situ* generating the **Int-II** complex as shown in Fig. 2F) to the binary system of CPA and $NaHCO_3$ resulted in the emergence of distinct ^{31}P NMR resonances at δ = 4.42 ppm and 5.64 ppm (no **2a**). These observations collectively demonstrate that (1) CPA undergoes base-mediated conversion to phosphate

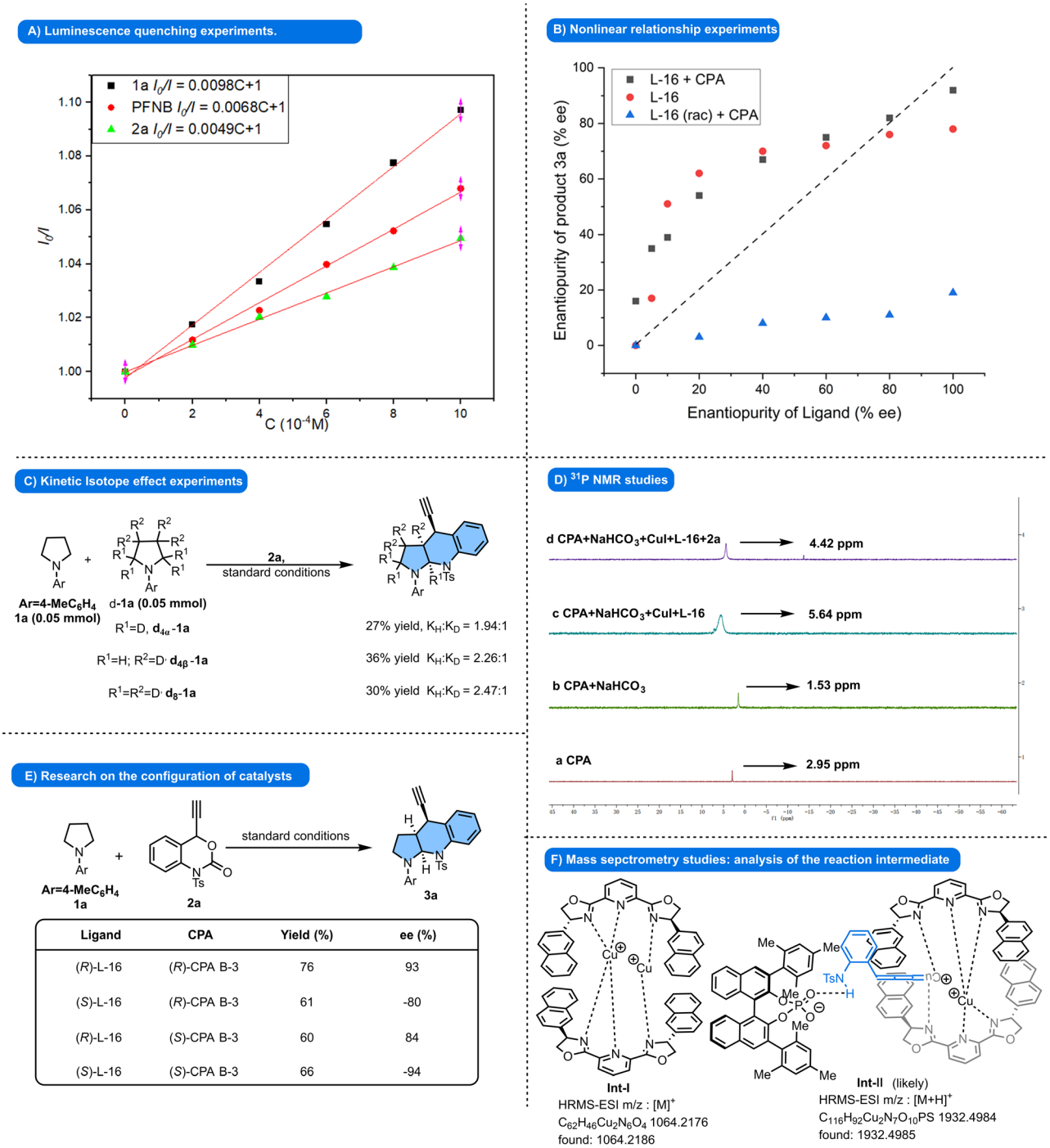

Ligand	CPA	Yield (%)	ee (%)
(*R*)-L-16	(*R*)-CPA B-3	76	93
(*S*)-L-16	(*R*)-CPA B-3	61	-80
(*R*)-L-16	(*S*)-CPA B-3	60	84
(*S*)-L-16	(*S*)-CPA B-3	66	-94

Fig. 2 Mechanistic studies. (A) Luminescence quenching experiments. (B) Nonlinear relationship experiments. (C) Kinetic isotope effect experiments. (D) ^{31}P NMR studies. (E) Research on the configuration of catalysts. (F) Mass spectrometry studies: analysis of the reaction intermediate.

species under catalytic conditions, and (2) synergistic coordination between the CPA-derived phosphate, **2a**, and the Cu/**L-16** complex generates a sterically defined chiral pocket (Fig. 2D). HR-MS analysis of the copper, ligand, CPA, and **2a** complex was conducted to identify potential reaction intermediates. Analysis of the collision-induced fragmentation of the reaction mixture revealed the formation of two key copper complexes, **Int-I** and **Int-II**, which are integral to the reaction pathway (Fig. 2F). It was envisioned that copper(I) coordinates with the chiral ligand and CPA, forming a Cu-CPA ion pair. The enantioselectivity of the reaction is facilitated by steric interactions between the copper ligand and CPA in **Int-II**, highlighting their critical role in stereochemical control. Intriguingly, cooperation between the (*R*)-Box ligand (**L-16**) and (*R*)-CPA **B-3** proved to be optimal for

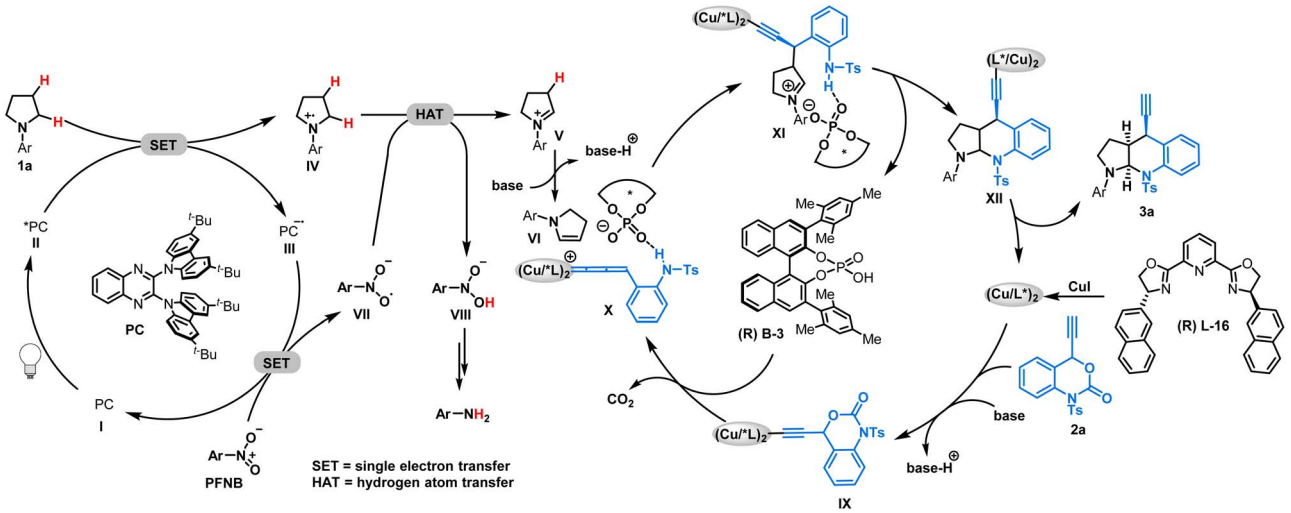

Fig. 3 Proposed reaction mechanism.

the enantiomeric ratio; however, an alternative combination of the (*R*)-Box ligand and (*S*)-CPA or (*S*)-Box ligand and (*R*)-CPA hampered the enantioselectivity in this migratory coupling (Fig. 2E).[27] Only when the configurations of the ligand and CPA matched did the reaction exhibit enhanced stereoselectivity, demonstrating the crucial interplay between these components.

Mechanism proposal

Based on experimental data, a dual catalytic cycle involving visible light, copper catalysis, and CPA was proposed for this asymmetric vicinal C(sp^3)–H difunctionalization (Fig. 3). The excited state of [^{t}Bu-DCQ] (**II**) is generated upon absorption of photons from the white light source. This high-energy intermediate (**II**) undergoes single-electron transfer (SET) with the amine substrate **1a**, producing a highly reducing [^{t}Bu-DCQ] radical anion (**III**) and the amine radical cation (**IV**). PFNB acts as an electron and hydrogen acceptor, regenerating ^{t}Bu-DCQ to its ground state and forming a highly activated nitrobenzene anion radical (**VII**). The interaction between **VII** and the amine radical cation **IV** effectively transforms **IV** into the desired enamine intermediate (**VI**). The copper catalyst, in the presence of a base, coordinates with substrate **2a** to form complex **IX**. This intermediate undergoes decarboxylation, yielding a highly reactive copper-allenylidene species (**X**). CPA interacts with copper-allenylidene species *via* H bonds and ion pairing, increasing enantioselectivity control. Cyclization of **X** and enamine intermediate **VI** produces intermediate **XII**, which undergoes copper elimination to furnish the final product **3a**.

Conclusions

In conclusion, we have reported an unprecedented asymmetric catalytic system employing a photoredox, Cu/chiral ligand and CPA to achieve vicinal C–H bond difunctionalization of saturated aza-heterocycles. This methodology offers efficient access to chiral ring-fused amine skeletons with excellent control over regioselectivity, diastereoselectivity, and enantioselectivity. The success of this reaction is attributed to the synergistic catalysis between the hydrogen bonding of the chiral phosphoric acid with the substrate and the additional counteranion interaction with the chiral copper cation. This approach effectively addresses the longstanding challenge of achieving enantioselective vicinal C–H bond formation in saturated cyclic amines. This work not only provides a powerful tool for synthesizing complex chiral ring-fused amine skeletons but also provides a solution to the problem that a single chiral catalyst cannot offer sufficient stereocontrol.

Author contributions

P. X., G. X., and T. X. conceived and supervised the project. T. X. and K. J. performed the synthetic experiments and analyzed the data. Y. C. participated in the discussions. T. X. wrote the manuscript. P. X. and G. X. revised and polished the manuscript. All authors discussed the results and commented on the manuscript.

Conflicts of interest

There are no conflicts to declare.

Data availability

CCDC 2413585 contains the supplementary crystallographic data for this paper.[28]

All experimental data associated with this work are available in the supplementary information (SI). Supplementary information is available. See DOI: https://doi.org/10.1039/d5sc06987d.

Acknowledgements

We are grateful to the NSFC (21871116, U22A20390, and 22371098), supported by the Xinjiang Uygur Autonomous

Region Science and Technology Department's project (No. Xincaihang [2023-211]), the Science and Technology Major Program of Gansu Province of China (22ZD6FA006, 23ZDFA015, and 23JRRA1512) the "111" program from the MOE of P. R. China (BP1221004), and the Syngenta PhD fellowship (W. Z.).

Notes and references

1 C. M. Marshall, J. G. Federice, C. N. Bell, P. B. Cox and J. T. Njardarson, *J. Med. Chem.*, 2024, **67**, 11622–11655.
2 J. Shearer, J. L. Castro, A. D. G. Lawson, M. MacCoss and R. D. Taylor, *J. Med. Chem.*, 2022, **65**, 8699–8712.
3 E. Vitaku, D. T. Smith and J. T. Njardarson, *J. Med. Chem.*, 2014, **57**, 10257–10274.
4 (*a*) K. R. Campos, A. Klapars, J. H. Waldman, P. G. Dormer and C. Chen, *J. Am. Chem. Soc.*, 2006, **128**, 3538–3539; (*b*) R. Guo, H. Xiao, S. Li, Y. Luo, J. Bai, M. Zhang, Y. Guo, X. Qi and G. Zhang, *Angew. Chem., Int. Ed.*, 2022, **61**, e202208232; (*c*) X. Shu, D. Zhong, Y. Lin, X. Qin and H. Huo, *J. Am. Chem. Soc.*, 2022, **144**, 8797–8806; (*d*) X. Shu, D. Zhong, Q. Huang, L. Huan and H. Huo, *Nat. Commun.*, 2023, **14**, 125–135; (*e*) J. Li, B. Cheng, X. Shu, Z. Xu, C. Li and H. Huo, *Nat. Catal.*, 2024, **7**, 889–899; (*f*) J. Zheng, H. Zhang, S. Kong, Y. Ma, Q. Du, B. Yi, G. Zhang and R. Guo, *ACS Catal.*, 2024, **14**, 1725–1732; (*g*) Z. Zhou, Y. Ke, R. Miao, F. Hu, X. Wang, Y. Ping, S. Xu and W. Kong, *Nat. Chem.*, 2025, **17**, 344–355.
5 A. S. K. Lahdenperä, P. D. Bacoș and R. J. Phipps, *J. Am. Chem. Soc.*, 2022, **144**, 22451–22457.
6 X. Ren, B. M. Couture, N. Liu, M. S. Lall, J. T. Kohrt and R. Fasan, *J. Am. Chem. Soc.*, 2023, **145**, 537–550.
7 (*a*) J. Xie, M. Rudolph, F. Rominger and S. K. Hashmi, *Angew. Chem., Int. Ed.*, 2017, **56**, 7266–7270; (*b*) E. Colson, J. Andrez, A. Dabbous, F. Dénès, V. Maurel, J. M. Mouesca and P. Renaud, *Commun. Chem.*, 2022, **5**, 57–68.
8 (*a*) X. Xia, X. Shu, K. Ji, Y. Yang, A. Shaukat, X. Liu and Y. Liang, *J. Org. Chem.*, 2010, **75**, 2893–2902; (*b*) R. K. Kawade, D. B. Huple, R. Lin and R. Liu, *Chem. Commun.*, 2015, **51**, 6625–6628; (*c*) X. Shi, Y. He, X. Zhang and X. Fan, *Adv. Synth. Catal.*, 2018, **360**, 261–266; (*d*) G. Xu, J. Xu, Z. Feng, H. Liang, Z. Wang, Y. Qin and P. Xu, *Angew. Chem., Int. Ed.*, 2018, **57**, 5110–5114; (*e*) W. Chen, A. Paul, K. Abboud and D. Seidel, *Nat. Chem.*, 2020, **12**, 545–550; (*f*) Y. He, Z. Zheng, Q. Liu, X. Zhang and X. Fan, *Org. Lett.*, 2020, **22**, 9053–9058; (*g*) T. Xiao, Y. Zhang, W. Hou, P. Yan, J. Hai, P. Xu and G. Xu, *Org. Lett.*, 2021, **23**, 8942–8946; (*h*) T. Feng, Z. Zhu, D. Zhang, S. Wang, R. Li, Z. Zhu, X. Zhang and Y. Qiu, *Green Chem.*, 2023, **25**, 2681–2689; (*i*) G. Kundu and T. H. Lambert, *J. Am. Chem. Soc.*, 2024, **146**, 1794–1798.
9 M. Hiersemann, Functions bearing two nitrogens, *Comprehensive Organic Functional Group Transformations 2*, Elsevier, Oxford, UK, 2005, pp. 411–441.
10 A. Numata, C. Takahashi, Y. Ito, T. Takada, K. Kawai, Y. Usami, E. Matsumura, M. Imachi, T. Ito and T. Hasegawa, *Tetrahedron Lett.*, 1993, **34**, 2355–2358.
11 J. Hájíček, J. Taimr and M. Buděšínský, *Tetrahedron Lett.*, 1998, **39**, 505–508.
12 R. H. Jiao, S. Xu, J. Y. Liu, H. M. Ge, H. Ding, C. Xu, H. L. Zhu and R. X. Tan, *Org. Lett.*, 2006, **8**, 5709–5712.
13 D. Crich and A. Banerjee, *Acc. Chem. Res.*, 2007, **40**, 151–161.
14 W. Xie, G. Jiang, H. Liu, J. Hu, X. Pan, H. Zhang, X. Wan, Y. Lai and D. Ma, *Angew. Chem., Int. Ed.*, 2013, **52**, 12924–12927.
15 D. Ju, Medicine for treating Alzheimer's disease, Chinese Pat., CN108553463, 2018.
16 D. Ju, Compound for treating Alzheimer's disease, Chinese Pat., CN 108484599, 2018.
17 D. Ju, Medicine containing 1-(5-bromo-2-fluorophenyl) piperidine-2-one for treating Alzheimer's disease, Chinese Pat., CN108358920, 2018.
18 B. I. Roman, S. Verhasselt and C. V. Stevens, *J. Med. Chem.*, 2018, **61**, 9410–9428.
19 M. A. Convery, A. P. Davis, C. J. Dunne and J. W. MacKinnon, *Tetrahedron Lett.*, 1995, **36**, 4279–4282.
20 G. S. Nandra, M. J. Porter and J. M. Elliott, *Synthesis*, 2005, **3**, 475–479.
21 A. J. P. Mortimer, S. P. Pang, A. E. Aliev, D. A. Tocher and M. J. Porter, *Org. Biomol. Chem.*, 2008, **6**, 2941–2951.
22 X. Liang, T. Y. Zhang, X. Y. Zeng, Y. Zheng, K. Wei and Y. D. Yang, *J. Am. Chem. Soc.*, 2017, **139**, 3364–3367.
23 E. D. Thorsett, E. E. Harris and A. A. Patchett, *J. Org. Chem.*, 1978, **43**, 4276–4279.
24 (*a*) H. Xu, Z. Lin, J. Bai, Y. Guo and S. Ma, *ACS Catal.*, 2024, **14**, 262–270; (*b*) L. Ding, J. Chen, H. Lu and Z. Shi, *J. Am. Chem. Soc.*, 2025, **147**, 28389–28398; (*c*) Z. Liao, Z. Li, M. Xiao, Y. Deng, Z. Ma, L. Zhou, G. Dai, X. Li, S. Wang, S. Chen, J. Li and S. Tang, *Nat. Commun.*, 2025, **16**, 7218–7231; (*d*) J. Lin, X. Dong, T. Li, N. Jiang, B. Tan and X. Liu, *J. Am. Chem. Soc.*, 2016, **138**, 9357–9360; (*e*) F. Wang, X. Dong, J. Lin, Y. Zeng, G. Jiao, Q. Gu, X. Guo, C. Ma and X. Liu, *Chem*, 2017, **3**, 979–990; (*f*) J. Lin, T. Li, J. Liu, G. Jiao, Q. Gu, J. Cheng, Y. Guo, X. Hong and X. Liu, *J. Am. Chem. Soc.*, 2019, **141**, 1074–1083; (*g*) Y. Cheng, J. Liu, Q. Gu, Z. Yu, J. Wang, Z. Li, J. Bian, H. Wen, X. Wang, X. Hong and X. Liu, *Nat. Catal.*, 2020, **3**, 401–410.
25 (*a*) T. Satyanarayana, S. Abraham and H. B. Kagan, *Angew. Chem., Int. Ed.*, 2009, **48**, 456–494; (*b*) Q. Wang, T. Li, L. Lu, M. Li, K. Zhang and W. Xiao, *J. Am. Chem. Soc.*, 2016, **138**, 8360–8363; (*c*) T. Satyanarayana, S. Abraham and H. B. Kagan, *Angew. Chem., Int. Ed.*, 2009, **48**, 456–494.
26 X. Xu, L. Peng, X. Chang and C. Guo, *J. Am. Chem. Soc.*, 2021, **143**, 21048–21055.
27 Z. Tao, W. Zhang, D. Chen, A. Adele and L. Gong, *J. Am. Chem. Soc.*, 2013, **135**, 9255–9258.
28 CCDC 2413585: Experimental Crystal Structure Determination, 2025, DOI: 10.5517/ccdc.csd.cc2m0jls.

